CHEMISTRY OF MATERIALS

The Dipole Moment Inversion Effects in Self-Assembled Nanodielectrics for Organic Transistors

Binghao Wang,[†] Gabriele Di Carlo,[†,‡] Riccardo Turrisi,[†,§] Li Zeng,[∥] Katie Stallings,[†] Wei Huang,[†] Michael J. Bedzyk,[∥] Luca Beverina,[*,§] Tobin J. Marks,[*,†,∥] and Antonio Facchetti[*,†]

[†]Department of Chemistry and the Materials Research Center, Northwestern University, 2145 Sheridan Road, Evanston, Illinois 60208, United States

[‡]Department of Chemistry, University of Milan, INSTM Research Unit, Via C. Golgi 19, 20133 Milano, Italy

[§]Materials Science Department, University of Milano-Bicocca, Via R. Cozzi 53, 20126, Milan, Italy

[∥]Applied Physics Program, Materials Science and Engineering Department and Material Research Center, Northwestern University, Evanston, Illinois 60208, United States

Supporting Information

ABSTRACT: We compare and contrast the properties of hybrid organic−inorganic self-assembled nanodielectrics (SANDs) based on alternating layers of solution-processed ZrO_x and either of two phosphonic acid-functionalized azastilbazolium π-units having opposite dipolar orientations. Conventional Zr-SAND and new inverted IZr-SAND are characterized by Kevin probe, optical spectroscopy, capacitance−voltage measurements, AFM, X-ray reflectivity, and electronic structure computation. The molecular dipolar orientation affects thin-film transistor (TFT) threshold and turn-on voltages for devices based on either p-channel pentacene or n-channel copper perfluorophthalocyanine. Specifically, Zr-SAND shifts threshold and turn-on voltages to more positive values, whereas IZr-SAND shifts them in the opposite direction. Capping these SANDs with $-SiMe_3$ groups enhances the effect, affording a 1.3 V difference in turn-on voltage for IZr-SAND vs Zr-SAND-gated organic TFTs. Such tunability should facilitate the engineering of more complex circuits.

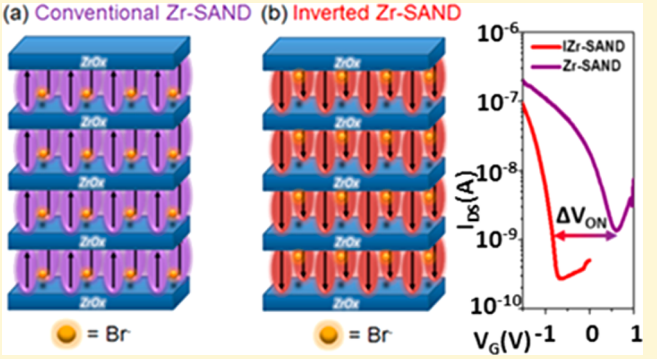

INTRODUCTION

In the growing field of organic electronics, a major challenge is providing reliable materials and methodologies for fabricating unconventional electronic devices.[1−6] Organic thin-film transistors (OTFTs) are of paramount interest, promising mechanical flexibility and facile solution processing.[7,8] The semiconducting layer has been by far the most investigated OTFT component, although the other materials and interfaces are also critical to performance. In particular, plastic electronics applications require that the gate dielectric evolve from a conventional rigid metal oxide film (e.g., SiO_2) to materials having a larger dielectric constant k, mechanical flexibility, and low voltage operation, as well as enabling fine-tuning of key device metrics such as threshold (V_{TH}) and turn-on voltage (V_{ON}).[9,10] Viable SiO_2 alternatives include metal oxides, electrolytes, self-assembled monolayers (SAMs) on metal oxides, and high-capacitance ultrathin/high-k polymers and polymer blends, each having their own strengths and limitations.[11−18]

Previously, we reported families of robust, structurally well-defined self-assembled nanodielectrics (SANDs) offering high capacitance, facile fabrication, and broad applicability to diverse semiconductors.[19,20] Our most advanced SANDs consist of alternating high-k metal oxide (ZrO_x or HfO_x) and highly polarizable, high-k **PAE** dipolar nanolayers (Figure 1a), all processed from solution under ambient.[21−23] To date, the effects, if any, of PAE dipolar orientation on the dielectric properties and OTFT response remain unknown. Here, we address this issue using an "inverted" **PAE** unit, named **IPAE**, to create a structurally inverted SAND (Figure 1b) and show from Kevin probe measurements, molecular orbital computations, and OTFT measurements that dipolar inversion occurs and that it affects, in an informative and useful way, the principal OTFT parameters relevant to circuit design and fabrication.[24,25]

EXPERIMENTAL SECTION

IPAE Synthesis and Characterization. All reagents are commercially available and were used without further purification unless otherwise stated. Anhydrous dichloromethane was distilled

Received: August 10, 2017
Revised: November 8, 2017
Published: November 10, 2017

DOI: 10.1021/acs.chemmater.7b03397
Chem. Mater. XXXX, XXX, XXX−XXX

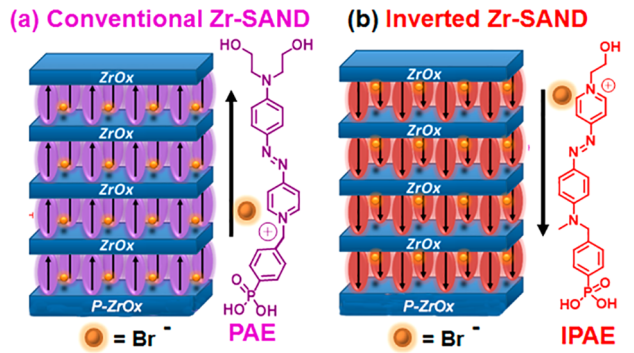

Figure 1. Dielectric stacks comprising four-chromophore/ZrO_x layers on top of the ZrO_x (p-ZrO_x) primer film. (a) Conventional Zr-SAND with a phosphonate π-electron (**PAE**) unit. (b) Inverted IZr-SAND with an inverted **PAE** (**IPAE**) π-unit.

from calcium hydride, whereas toluene was distilled from Na/benzophenone. Unless otherwise stated, all reactions were carried out under N_2 using standard Schlenk line techniques. Details of IPAE synthesis are given in the Supporting Information. UV−vis spectra were recorded on a Varian Cary 50 Scan UV−vis spectrophotometer. Microwave enhanced reactions were performed in a CEM Discover Instrument working under Dynamic conditions. NMR spectra were recorded on a Varian Unity Plus 500 (500 MHz, room temperature) spectrometer, and chemical shifts are referenced to TMS for ^1H and internally calibrated by the spectrometer for ^{31}P.

SAND Film Growth. ZrO_x solutions for the deposition of ZrO_x layers were prepared by dissolving 93.2 mg of $ZrCl_4$ (Sigma-Aldrich) in 4.0 mL of absolute ethanol, affording a 0.1 M solution. After 5 min of stirring, 300 mg of 68% wt./wt. HNO_3 was added and the solution was heated at 60 °C for 3 h, then aged at room temperature for 12 h. From this mother solution, 0.01 and 0.02 M solutions were prepared by dilution with ethanol for future use. The substrates (glass or n^{+2}-Si/native SiO_2) were cleaned by sonication in acetone, hexane, and ethanol for 5 min, followed by air plasma cleaning (400−500 mTorr) for 5 min. Growth of the dielectric stacks was carried out in a Class-10 HEPA filtered laminar flow clean hood (NuAire) to minimize contamination. All solutions were filtered through 0.2 μm Teflon syringe filters. Growth of Zr-SAND and IZr-SAND films was carried out in the following these steps: Step 1 (ZrO_X-Primer): The ZrOx primer layer was prepared by spin-coating the 0.02 M precursor solution at 5000 rpm for 30 s, then baking the coated substrate at 220 °C for 20 min. Step 2 (PAE/IPAE Self-Assembly): The organic molecular layer was self-assembled on the surface by immersing the primer-coated substrate in a 3 mM methanol solution of the azastilbazolium reagent of interest, PAE for Zr-SAND and IPAE for IZr-SAND, for 1 h at 60 °C.[26] The films were then cleaned by sonication in methanol for 5 s using two different methanol baths. Step 3 (ZrO_x-Capping): The capping layer was fabricated by spin-coating the 0.01 M precursor solution at 5000 rpm for 30 s, then baking at 220 °C for 20 min. The last two steps (self-assembly + ZrO_x capping) were repeated in sequence to achieve the desired number of SAND layers. The HMDS-capped cZr-SAND and cIZr-SAND films were fabricated by spin-coating pure HMDS on top of 4 layers Zr-SAND and IZr-SAND films. (5000 rpm, 30 s), followed by annealing at 130 °C for 20 min.

SAND Film Characterization. X-ray reflectivity (XRR) was performed on an 18 kW Rigaku ATXG diffractometer workstation with Cu Kα radiation (λ = 1.54 Å). The reflectivity data for the IZr-SAND thin films are plotted as a function of momentum transfer ($Q = 4\pi \sin(\theta)/\lambda$) and fitted with the Motofit/Igor software package to extract the film thickness and electron density profile. Kelvin Probe measurements were carried out on an Ambient Kelvin Probe System (KP technology, USA). The humidity was ~22%. The reference electrode was gold. SAND film UV−vis spectra were recorded on a Varian Cary 50 Scan spectrophotometer. FT-IR spectra were collected on a Nexus 870 spectrometer (Thermo Nicolet) with a single reflection horizontal ATR accessory having a diamond ATR crystal fixed at a 45° incident angle.

Electrical Measurements on SAND Films. To fabricate metal−insulator−semiconductor capacitors, gold contacts were thermally evaporated at a 0.3 Å/s rate from a base pressure of 3×10^{-6} Torr through 200 μm × 200 μm shadow masks. MIS characterization was performed under ambient conditions using an Agilent B1500A semiconductor parameter analyzer. Leakage current density vs voltage ($J-V$) curves, areal capacitance vs voltage ($C-V$) curves, and areal capacitance vs frequency ($C-f$) curves were recorded under ambient conditions using a flexible tungsten 1 μm whisker probe (SE-SM, Signatone) as a cathode and a beryllium−copper alloy probe (SE-BC, Signatone) as an anode. $C-V$ curves were tested at 10 kHz. The multilayer dielectric in the n^{+2}-Si/Zr-SAND [primer ZrO_2/(PAE/capping $ZrO_2)_n$, n (number of bilayers) = 1, 2, 3, and 4]/Au MIS devices can be modeled as capacitors in series, according to eq 1. Here, SiO_2 is the native oxide on the Si wafer, p-ZrO_2 is the ZrO_2 primer layer,

$$\frac{1}{C_i} = \left(\frac{1}{C_{SiO_2}} + \frac{1}{C_{p\text{-}ZrO_2}}\right) + n\cdot\left(\frac{1}{C_{Org}} + \frac{1}{C_{c\text{-}ZrO_2}}\right) \quad (1)$$

c-ZrO_2 is the ZrO_2 capping layer, and Org is the PAE or IPAE layer. The capacitances of the native oxide and ZrO_2 primer layer on the n^{+2}-Si bottom electrode are 2236 and 4425 nF/cm^2, respectively, assuming a 1.5 nm thick SiO_2 (k = 3.9) and 2 nm thick ZrO_2 layer (k = 10).

Organic Thin-Film Transistor Fabrication and Characterization. Pentacene (P5, 99%, Sigma-Aldrich) and copper perfluorophthalocyanine (F_{16}CuPc, 98%, TCI Chemicals) were sublimed twice (base pressure: 7.0×10^{-6} Torr) in a three-zone sublimer prior to use. Temperatures for pentacene: 290, 275, 230 °C. Temperatures for F16PcCu: 460, 400, 300 °C. Semiconductor films (50 nm thick) were patterned during thermal evaporation (0.1 Å/s, base pressure 3.5×10^{-6} Torr) through 5 mm × 8 mm shadow masks. The substrates were kept at 25 °C for P5 evaporation and at 125 °C for F_{16}CuPc evaporation. OTFT fabrication was completed by thermal evaporation (50 nm, 0.3 Å/s, base pressure 3×10^{-6} Torr) of gold contacts (W = 5 mm, L = 100 μm). Transfer and output plots were recorded using an Agilent B1500A semiconductor parameter analyzer. Carrier mobilities (μ) were evaluated in the saturation regime with a conventional metal−oxide−semiconductor field-effect transistor model. The capacitance of Zr-SAND/cZr-SAND and IZr-SAND/cIZr-SAND used for mobility calculations are 465/352 and 503/394 nF cm^{-2} (measured at 10^4 Hz), respectively.

RESULTS AND DISCUSSION

Here, we first report the design and synthesis of the new IPAE building block for nanodielectric films, then fabricate in parallel, conventional Zr-SAND and inverted IZr-SAND films. These dielectric films are characterized by several methods including optical, electrical, and morphological measurements. In addition, the dipolar inversion is investigated by Kevin probe techniques and DFT computation, corroborating inversion of the dipole. Finally, p-/n-channel OTFTs are fabricated and the device performance parameters discussed in detail, including how they vary with SAND and organic semiconductor microstructure.

Synthetic Strategy for Inverted SANDs. The design and synthesis of an inverted **PAE** analogue having similar connectivity, **IPAE**, is shown in Scheme 1. Note that, although the π-conjugated azastilbazolium cores of **PAE** and **IPAE** are identical, there are minor differences in the structures such as larger distance between the phenylphosphonic acid portion and the core (1 atom in **PAE** and 2 atoms in **IPAE**) and, more evident, two hydroxylethyl fragments in the latter versus one in the former structure. However, the hydroxyethyl group is not the anchoring point of the chromophore to the surface but is

DOI: 10.1021/acs.chemmater.7b03397
Chem. Mater. XXXX, XXX, XXX−XXX

Scheme 1. Synthesis of Inverted SAND Building Block IPAE

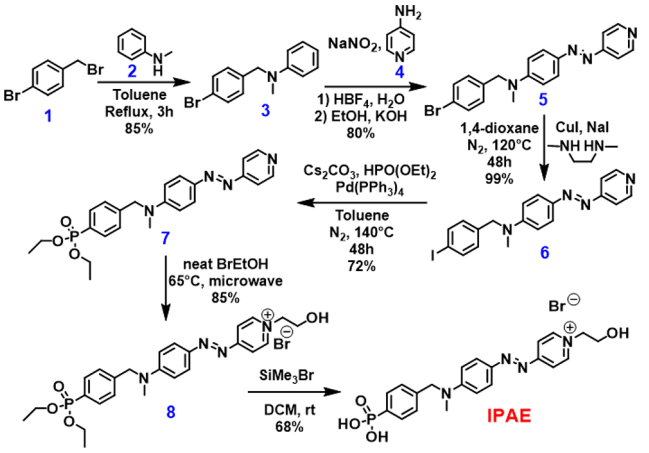

simply used to achieve good chemical adhesion to the overlying ZrO_x layer. More importantly, it does not drive the self-assembly process as judged from the kinetics of **PAE**/**IPAE** absorption, which are governed by the phosphonic acid fragment and are identical for the two systems (*vide infra*).

The **IPAE** synthesis begins with the nucleophilic attack of *N*-methylaniline **2** on the benzylic position of 4-bromobenzyl bromide **1**. The resulting amine **3** is then employed in diazo coupling with pyridine moiety **4**. Traditional approaches were unsuccessful to afford **5** with acceptable yields.[27−30] However, the generation of diazonium salt by aqueous HBF_4 + $NaNO_2$ produces the *N*-asymmetric azabenzenes in high yields.[31] The structure of **5** was confirmed by single-crystal diffraction (see the Supporting Information). Surprisingly, functionalization of **5** with a diethyl-phosphonate group was unsuccessful via either Pd-catalyzed Hirao or Ni-catalyzed coupling.[32,33] Thus, Finkelstein halide exchange was used to obtain iodo derivative **6**, which was then converted into phosphonate **7** under Hirao conditions. Alkylation of **7** to give **8** in neat 2-bromoethanol under microwave irradiation, followed by phosphonic ester cleavage with Me_3SiBr, affords phosphonic acid **IPAE** in good yield. Characterization by elemental analysis, NMR, and single-crystal diffraction of **IPAE** and synthetic intermediates are presented in Figures S1−S7 and Tables S1−S7. As noted above, the **IPAE** double hydroxyethyl group is not the chromophore anchoring point to the surface but is used to achieve good chemical adhesion to the top ZrO_x layer.

Figure 2a shows **IPAE** and **PAE** optical spectra in methanol solution. The former features a hypsochromic shift of ∼20 nm in λ_{max} and half the molar extinction coefficient ε of **PAE** (Table 1). This result likely reflects the different roles of the phosphonic acid electron-withdrawing residue in the two molecules. Thus, the $PO(OH)_2$ moiety increases the "pull" character of the electron-poor pyridinium moiety in **PAE**, increasing the oscillator strength along the molecular axis and red-shifting λ_{max}. In contrast, the electron-withdrawing effect in **IPAE** decreases the charge density on the amine "push" nitrogen, thus decreasing the total oscillator strength and the donor−acceptor coupling. Note that the presence of a phosphonic acid (pK_{a1} ∼ 1−2) and an azo bridge base (pK_a ∼ 3−4) in the same molecule imparts halochromic properties, typical of aromatic azo compounds such as the pH indicator methylorange.[34,35] Concentrated polar **IPAE** solutions (>0.1 M) appear red, while dilution increases the pH and λ_{max} shifts toward that observed in Figure 2a.

SAND Film Characterization. UV−vis-monitored kinetic measurements (Figure 2b) indicate that **PAE** and **IPAE** have comparable grafting rates on the ZrO_x surface of glass/ITO/ZrO_x substrates and reach maximum SAM densities after ∼60 min at 60 °C (data points normalized to ε). IZr-SAND fabrication of *n*-bilayers (from 1 to 4) is similar to that reported for conventional Zr-SANDs, with the IZr-SAND optical absorption on glass at 547 nm increasing linearly with the number of bilayers, and FT-IR spectra clearly demonstrating

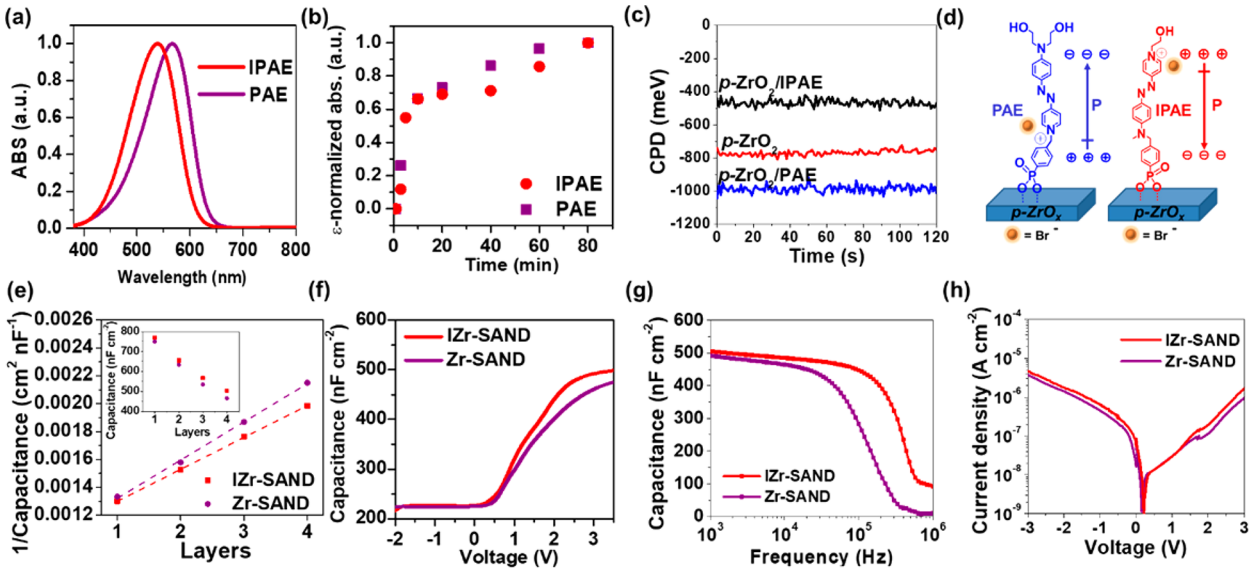

Figure 2. (a) Normalized optical absorption spectra of **PAE** and **IPAE** in MeOH. (b) Optical spectroscopic data as a function of monolayer self-assembly time. (c) Contact potential difference (CPD) for p-ZrO_x/Si, PAE/p-ZrO_x/Si, and IPAE/p-ZrO_x/Si films. (d) Illustration of the different polarization directions for PAE and IPAE. (e) Reciprocal of capacitance vs the number of SAND layers with the corresponding linear fit indicated by the broken lines; Inset: Corresponding areal capacitance vs the number of layers. Representative (f) *C*−*V* curves (measured at 10^4 Hz), (g) *C*−*f* curves (measured at 3.5 V), and (h) *J*−*V* plots for Zr-SAND and IZr-SAND (n = 4). In all MIS measurements, the metal is grounded.

DOI: 10.1021/acs.chemmater.7b03397
Chem. Mater. XXXX, XXX, XXX−XXX

Table 1. Optical Properties of PAE Derivatives and Dielectric Properties of IZr-SAND and Zr-SAND Stacks with Different Numbers of (Bi)layers

	optical		capacitance (nF cm^{-2})				d_{XRR} (nm)[a]	
chromophore/dielectric	λ_{MAX} (nm)	ε (L cm^{-1} mol^{-1})	1 Layer	2 Layers	3 Layers	4 Layers	4 Layers	k_{org}[b]
IPAE/IZr-SAND	547	5.30 × 10^4	770	655	566	503	12.2 nm	13
PAE/Zr-SAND	567	2.59 × 10^4	750	633	535	465	12.1 nm	9

[a] d_{XRR} = thickness established by X-ray reflectivity. [b] k_{org} is the dielectric constant of **PAE** or **IPAE**.

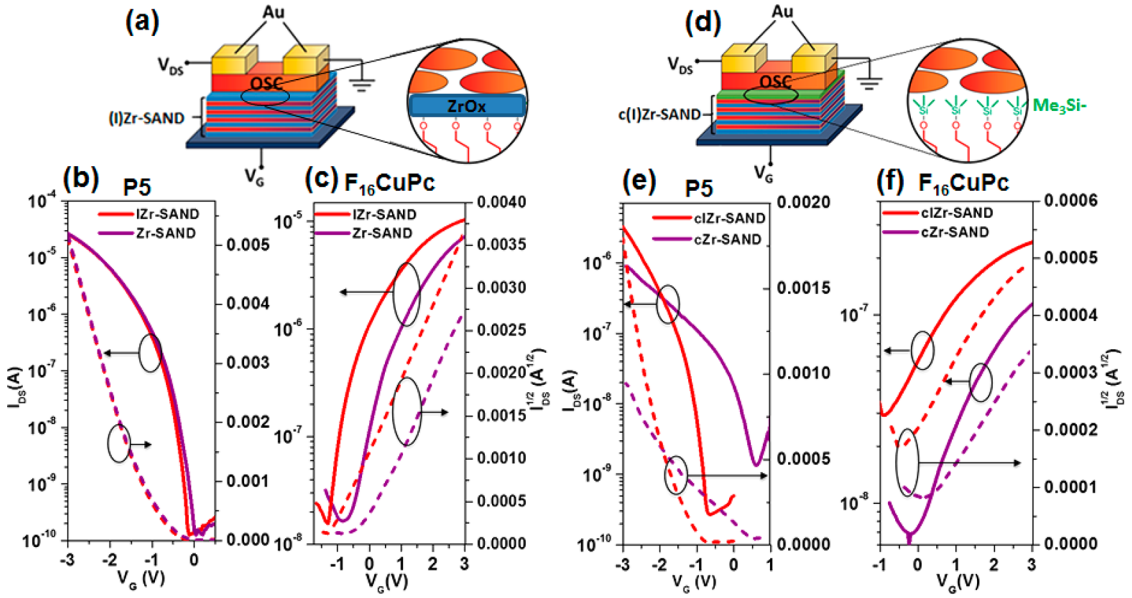

Figure 3. (a) Schematic of OTFTs fabricated on Zr-SAND and IZr-SAND. Representative transfer plots (V_{DS} = ±3 V) for (b) P5 OTFTs and (c) F_{16}PcCu OTFTs on Zr-SAND and IZr-SAND. (d). Schematic of OTFTs fabricated on TMS-capped cZr-SAND and cIZr-SAND. Representative transfer plots (V_{DS} = ±3 V) for (e) P5 OTFTs and (f) F_{16}PcCu OTFTs on cZr-SAND and cIZr-SAND. The off-current variations (Figure S18) may originate from both the different semiconductor film morphologies and the slightly larger gate leakage for c(I)Zr-SAND vs the (I)Zr-SAND films.

the CH_2 stretching (2920 and 2850 cm^{-1}) and arene ring vibrational modes (1580, 1230, and 878 cm^{-1}) (Figure S8).

Before IZr-SAND fabrication and characterization, the inversion in the surface dipole was assessed experimentally by Kelvin probe analysis and theoretically by DFT calculations. The Kelvin probe measures the contact potential difference (CPD) between a reference surface (gold) and the sample.[36] Thus, the CPD values (Figure 2c) of PAE/Primer ZrO_x (PAE/p-ZrO_x) (∼ −983 meV) is more negative than that of IPAE/Primer ZrO_x (IPAE/p-ZrO_x) (∼ −463 meV), with that of the primer ZrO_x located in between (∼ −770 meV). This result substantiates dipole inversion and is in agreement with the pictorial orientation toward the surface (Figure 2d), thus facilitating electron extraction and decreasing the CPD value. Furthermore, the different directions of PAE and IPAE SAM dipole moments is supported by MO computations (Figure S9, Table S8, *vide infra*). Together, these data argue that the chromophore components of the SAND/ISANDs should produce opposite built-in electric fields.[37,38]

SAND Dielectric and Electrical Properties. To assess the dielectric properties of these hybrid ZrO_x−azastilbazolium stacks, SANDs were fabricated on n^{+2}-Si substrates using **PAE** (Zr-SAND) and **IPAE** (IZr-SAND), following an iterative process of sol−gel ZrO_x spin-casting, thermally assisted densification at 220 °C in air, and immersion-grafting in methanol (details in the SI and AFM images in Figure S10). X-ray reflectivity of the 4-Layer IZr-SAND and Zr-SAND demonstrate almost identical thickness, 12.2 and 12.1 nm, respectively (Table 1, Figure S8). Metal−insulator−semiconductor (MIS) capacitors were fabricated by gold electrode thermal deposition (device area = 200 μm × 200 μm) on Zr-SAND and IZr-SAND (details in the SI). The capacitance shows linear dependence on the number of layers (n) (Figures 2e and S11), confirming the regular multilayer structures of the **PAE**- and **IPAE**-based SANDs. These data indicate that the capacitance values of the IZr-SANDs are slightly larger than those of the corresponding Zr-SANDs, attributed to the slightly different molecular structure and opposite the built-in polarization orientation (Table 1).

Regarding capacitance response with voltage (Figures 2f and S11), note the following: (a) The effects of the **PAE** vs **IPAE** structure on the dielectric stack capacitance manifest themselves in slightly higher values for IZr-SAND stacks vs Zr-SAND stacks and by different dC/dV values in the accumulation regime (Figure S12); these data can be interpreted by considering that, during the capacitance measurement, the molecular dipole in IZr-SAND is oriented with the applied field effectively promoting positive/negative charge localizations at the top/bottom interfaces (Figure 2d). (b) The voltage onset of accumulation is more negative for IZr-SANDs [−400 to +300 mV] than for Zr-SANDs [−100 to +250 mV], which is in agreement with the different built-in polarization of the two nanodielectric types (Table S9).[39] Figure 2g shows the C−f curves for 4-layer Zr-SAND and IZr-SAND dielectrics, indicating that the latter exhibit stable capacitance to a greater frequency range (1 × 10^5 Hz) than the

DOI: 10.1021/acs.chemmater.7b03397
Chem. Mater. XXXX, XXX, XXX−XXX

Table 2. Electrical Parameters for OTFTs Fabricated with the Indicated Four-Layer ZrO_x Based SANDs[a]

	OTFT structure of Figure 3a[b]				OTFT structure of Figure 3d[c]			
	P5 (p-channel)		F_{16}PcCu (n-channel)		P5 (p-channel)		F_{16}PcCu (n-channel)	
OTFT metrics	Zr-SAND	IZr-SAND	Zr-SAND	IZr-SAND	cZr-SAND	cIZr-SAND	cZr-SAND	cIZr-SAND
μ ($cm^2\ V^{-1}\ s^{-1}$)	0.44 ± 0.04 (0.58)	0.55 ± 0.05 (0.69)	0.051 ± 0.003 (0.066)	0.055 ± 0.002 (0.070)	0.032 ± 0.004 (0.05)	0.17 ± 0.01 (0.20)	~0.002	~0.001
I_{ON}/I_{OFF}	$\sim 10^5$	$\sim 10^5$	$\sim 10^3$	$\sim 10^3$	$\sim 10^3$	$\sim 10^4$	10^2	~10
V_{TH} (V)	−0.95 ± 0.0.01	−1.00 ± 0.01	−0.30 ± 0.08	−0.80 ± 0.06	−1.00 ± 0.02	−1.65 ± 0.03	~-0.5[d]	~-2[d]
ΔV_{TH} (mV)	−50		−500		−650		~ −1500	
V_{ON} (V)	0 ± 0.01	−0.15 ± 0.02	−0.8 ± 0.01	−1.3 ± 0.02	0.65 ± 0.05	−0.65 ± 0.04	~-0.1[d]	~-0.9[d]
ΔV_{ON} (mV)	−150		−500		−1300		~ −700	
SS (V/dec)	0.18 ± 0.01	0.18 ± 0.02	1.26 ± 0.04	1.20 ± 0.03	0.40 ± 0.05	0.20 ± 0.02	~2[d]	~2[d]

[a]Values represent the average of 10+ devices and are reported with relative uncertainties; the mobility values in parentheses are the maximum values. [b]ZrO_x-capped four-layer Zr-SANDs and IZr-SANDs. [c]Me_3Si-capped four-layer cZr-SANDs and cIZr-SANDs. [d]Approximate due to the low μ values and I_{ON}/I_{OFF} ratios.

former (3×10^4 Hz). The leakage currents of 4-layer Zr-SAND and IZr-SAND (Figure 2f) are ~1−2 × 10^{-6} A cm^{-2} at 3 V, albeit those of IZr-SAND are statistically slightly larger, comparable to other ZrO_x- and HfO_x-based **PAE** dielectrics.[20,23]

Thin-Film Transistors. To probe dipole inversion effects on charge transport and V_{TH}/V_{ON}, 4-layer IZr-SAND and Zr-SAND stacks were used to fabricate bottom-gate, top-contact OTFTs by evaporating pentacene (P5, p-type) or Cu perfluorophthalocyanine (F_{16}PcCu, n-type) films and Au S/D contacts (W = 5 mm, L = 100 μm; full details in the SI). The OTFT architecture is shown in Figure 3a, while the associated transfer plots measured at ±3 V are in Figure 3b,c. Key TFT parameters are summarized in Table 2. P5 and F_{16}PcCu TFTs carrier mobilities on both types of SANDs are large (0.4−0.6 and 0.05−0.06 $cm^2\ V^{-1}\ s^{-1}$, respectively)—greater than previously reported for similar OTFT achitectures.[16] Note that, since semiconductor morphology is not affected by the SAND type (*vide infra*), carrier mobility in saturation should and does remain similar for the two SANDs. However, importantly, both semiconductors exhibit a negative V_{TH}/V_{ON} shift, from −50 to −700 mV, on going from Zr-SAND to IZr-SAND (Table 2). To verify that these shifts are not morphology-related, AFM images of P5 and F_{16}PcCu films on IZr- and Zr-SAND were recorded and indicate no major differences (Figure S13), exhibiting typical vapor-deposited P5 and F_{16}PcCu crystallites. Note that, on average, the V_{ON} shift (−150 mV for P5 and −500 mV for F_{16}PcCu) is larger than the V_{TH} shift [−50 mV for P5 and −300 mV for F_{16}PcCu], in agreement with other studies investigating effect polarity and dipole orientation effects on the transport characteristics of organic semiconductors.[40,41] Also, comparing the V_{TH} of P5 OTFTs based on 3L- and 4L-IZr-SAND, note that the V_{TH} shifts positive from 3L to 4L-SANDs (Figure S14), demonstrating the more prominent dipole effect of the latter.

Interestingly, Kelvin probe measurements (Figure S15) indicate that the CPD values of the PAE/p-ZrO_x or IPAE layer capped with a ZrO_x film (structures equivalent to a 1L Zr-SAND/IZr-SAND films) are almost identical to the primer ZrO_x (p-ZrO_x), suggesting that the surface potential difference between the two types of chromophores is moderated on capping. To understand whether there is a dampening effect on V_{TH}/V_{ON} due to the uppermost ZrO_x capping layer, OTFTs were fabricated minus the top ZrO_x layer but with Me_3Si- capping of the exposed organic hydroxyl groups to yield cZr-SAND and cIZr-SAND (Figure 3d). The device data (transfer plots in Figure 3e,f) indicate two interesting trends on replacing the ~1 nm ZrO_x cap with Me_3Si− groups. The leakage currents (Figure S16a) of cZr-SAND and cIZr-SAND are ~2−4 × 10^{-6} A cm^{-2} at −3 V, slightly higher than those of the corresponding Zr-SAND and IZr-SAND. The C−f plots (Figure S16b) exhibit obvious frequency dependence even at low frequencies, indicating Me_3Si− capping cannot prevent ion motion in **PAE** and **IPAE** layers. Note that a clear onset voltage difference in the capacitance measurements can be detected by measuring cZr-SAND vs cIZr-SAND (−0.09 vs 0.16 V), thus eliminating the dampening effect from ZrO_x capping layer (Figure S16c). With regard to the OTFT performance, first, the carrier mobilities of both semiconductors fall [0.2−0.03 $cm^2\ V^{-1}\ s^{-1}$ for P5 and ~10^{-3} $cm^2\ V^{-1}\ s^{-1}$ for F_{16}PcCu] as a result of non-optimal semiconductor film morphology (Figure S17), indicated by far smaller grains than in the ZrO_x-capped SANDs. Specifically, the F_{16}PcCu AFM phase images show sub-50 nm crystallites with abundant grain boundaries, and complete loss of contiguity in the semiconducting layer. We infer that the different substrate surface energies and closer proximity of the molecular dipole to the interface may induce a non-optimal semiconductor growth morphology, particularly near the dielectric surface in the channel region. Second, and most important, the dipole inversion-related V_{TH}/V_{ON} shifts increase significantly as the result of the closer coupling between the dipolar component of the SAND stack and the semiconductor. Thus, in the P5 OTFTs, replacing the ZrO_x capping layer with Me_3Si− induces significant dipole inversion V_{TH} and V_{ON} shifts of −650 and −1300 mV, respectively. For the F_{16}PcCu-based devices, both V_{TH}/V_{ON} shifts are ~ −700 mV—larger than that measured for the ZrO_x-capped SANDs; however, the V_{TH} shift is not as dramatic as for P5. This result may reflect the limited accuracy of the OTFT parameters for the low-mobility F_{16}PcCu devices on cIZr-SAND as well as the limited significance of V_{TH} shifts when comparing devices with very different electrical characteristics,[40,42−44] as for P5 OTFTs on the same dielectric. Note also that the slower P5 turn-on (larger subthreshold swing) on Zr-SAND and its incomplete saturation may obscure the comparison between these different gate dielectrics.

The direction of the present V_{TH}/V_{ON} shifts parallels those of other SAM dipole inversion experiments,[42,45,46] consistent with an **IPAE** dipole inversion vs **PAE**. Using the cIZr-SAND versus IZr-SAND ΔV_{ON} parameters, it should be possible to estimate the dipole direction from $\Delta V = NP_\perp/\varepsilon_0 k$, where N and k are the surface density and the dielectric constants of the organic

DOI: 10.1021/acs.chemmater.7b03397
Chem. Mater. XXXX, XXX, XXX−XXX

SAMs (Table 1), and $P_\perp$ is the molecular dipole moment along the molecular long axis. Taking into account the presence of four organic layers, $P_\perp$ along the substrate normal for **IPAE** and **PAE** layers is therefore estimated to be +2.00 D and −1.45 D, respectively. A positive sign indicates dipolar orientation from the Si substrate to the film surface, in agreement with dipole inversion as depicted in Figure 1.[46] Note that these results are in accord with the $P_\perp$ found here for **IPAE** (+0.70 D) and **PAE** (−3.04 D), estimated by combining long-period X-ray standing wave experiments[47] and DFT computations (Figure S9), as well as previous identification of gate dielectric dipolar effects in very different materials.[10,45] Note that the counterion should also affect the chromophore polarizability and we are now exploring other anions.

■ CONCLUSIONS

A "dipole inverted" phosphonic acid-functionalized azastilbazolium molecule (**IPAE**) was synthesized and characterized, and the resulting IZr-SAND properties were investigated by a battery of techniques. It is shown that the threshold and turn-on voltages of p- and n-type OTFTs based on ZrO_x-derived SANDs can be tuned by manipulating the phosphonate dipolar orientation and proximate dielectric functionality. We believe that SAND dipole modulation, along with new semiconductor design and device engineering, can further advance optoelectronic device performance. Future efforts include exploration of different counterions, whose structure can greatly impact the overall dipole moment strength and direction, as well as fabricating these structures in a cleanroom and using all-patterned layers for detailed statistical analysis.

■ ASSOCIATED CONTENT

Supporting Information

The Supporting Information is available free of charge on the ACS Publications website at DOI: 10.1021/acs.chemmater.7b03397.

Full experimental procedures, AFM images, NMR spectra, UV−vis spectra, capacitance data, crystallographic data, and DFT computations (PDF)

■ AUTHOR INFORMATION

Corresponding Authors

*E-mail: a-facchetti@northwestern.edu (A.F.).
*E-mail: t-marks@northwestern.edu (T.J.M.).
*E-mail: luca.beverina@mater.unimib.it (L.B.).

ORCID

Gabriele Di Carlo: 0000-0002-8782-7945
Li Zeng: 0000-0001-6390-0370
Wei Huang: 0000-0002-0973-8015
Michael J. Bedzyk: 0000-0002-1026-4558
Luca Beverina: 0000-0002-6450-545X
Tobin J. Marks: 0000-0001-8771-0141

Funding

This work was supported by the BSF (AGMT-2012250), the MRSEC program of the National Science Foundation (DMR-1121262), and ONR (MURI N00014-11-1-0690). A.F. thanks the Shenzhen Peacock Plan project (KQTD20140630110339343) for financial support. This work made use of the J. B. Cohen X-ray Diffraction Facility, EPIC facility, Keck-II facility, and SPID facility of the NUANCE Center at Northwestern U., which received support from the Soft and Hybrid Nanotechnology Experimental (SHyNE) Resource (NSF NNCI-1542205); the MRSEC program (NSF DMR-1121262) at the Materials Research Center; the International Institute for Nanotechnology (IIN); the Keck Foundation; and the State of Illinois, through the IIN.

Notes

The authors declare no competing financial interest.

■ ACKNOWLEDGMENTS

We specially thank Mr. Bo Fu and Professor Mark A. Ratner of Northwestern University for the DFT computations.

■ REFERENCES

(1) Xu, Y.; Sun, H.; Shin, E. Y.; Lin, Y. F.; Li, W. W.; Noh, Y. Y. Planar-Processed Polymer Transistors. *Adv. Mater.* **2016**, *28*, 8531.

(2) Shankar, S.; Lahav, M.; van der Boom, M. E. Coordination-Based Molecular Assemblies as Electrochromic Materials: Ultra-High Switching Stability and Coloration Efficiencies. *J. Am. Chem. Soc.* **2015**, *137*, 4050.

(3) Osaka, I.; Takimiya, K. Backbone orientation in semiconducting polymers. *Polymer* **2015**, *59*, A1.

(4) Zhang, L.; Colella, N. S.; Cherniawski, B. P.; Mannsfeld, S. C. B.; Briseno, A. L. Oligothiophene Semiconductors: Synthesis, Characterization, and Applications for Organic Devices. *ACS Appl. Mater. Interfaces* **2014**, *6*, 5327.

(5) Stalder, R.; Mei, J. G.; Graham, K. R.; Estrada, L. A.; Reynolds, J. R. Isoindigo, a Versatile Electron-Deficient Unit For High-Performance Organic Electronics. *Chem. Mater.* **2014**, *26*, 664.

(6) Matsidik, R.; Luzio, A.; Askin, Ö.; Fazzi, D.; Sepe, A.; Steiner, U.; Komber, H.; Caironi, M.; Sommer, M. Highly Planarized Naphthalene Diimide−Bifuran Copolymers with Unexpected Charge Transport Performance. *Chem. Mater.* **2017**, *29*, 5473.

(7) D'Innocenzo, V.; Luzio, A.; Abdalla, H.; Fabiano, S.; Loi, M. A.; Natali, D.; Petrozza, A.; Kemerink, M.; Caironi, M. Two-dimensional charge transport in molecularly ordered polymer field-effect transistors. *J. Mater. Chem. C* **2016**, *4*, 11135.

(8) Mukhopadhyay, T.; Puttaraju, B.; Senanayak, S. P.; Sadhanala, A.; Friend, R.; Faber, H. A.; Anthopoulos, T. D.; Salzner, U.; Meyer, A.; Patil, S. Air-Stable *n*-channel Diketopyrrolopyrrole Diketopyrrolopyrrole Oligomers for High Performance Ambipolar Organic Transistors. *ACS Appl. Mater. Interfaces* **2016**, *8*, 25415.

(9) Kirsch, P. D.; Sivasubramani, P.; Huang, J.; Young, C. D.; Quevedo-Lopez, M. A.; Wen, H. C.; Alshareef, H.; Choi, K.; Park, C. S.; Freeman, K. Dipole model explaining high-*k*/metal gate field effect transistor threshold voltage tuning. *Appl. Phys. Lett.* **2008**, *92*, 092901.

(10) Zschieschang, U.; Ante, F.; Schlorholz, M.; Schmidt, M.; Kern, K.; Klauk, H. Mixed Self-Assembled Monolayer Gate Dielectrics for Continuous Threshold Voltage Control in Organic Transistors and Circuits. *Adv. Mater.* **2010**, *22*, 4489.

(11) Wang, B.; Yu, X.; Guo, P.; Huang, W.; Zeng, L.; Zhou, N.; Chi, L.; Bedzyk, M. J.; Chang, R. P. H.; Marks, T. J.; Facchetti, A. Solution-Processed All-Oxide Transparent High-Performance Transistors Fabricated by Spray-Combustion Synthesis. *Adv. Electron. Mater.* **2016**, *2*, 1500427.

(12) Kim, S. H.; Hong, K.; Xie, W.; Lee, K. H.; Zhang, S.; Lodge, T. P.; Frisbie, C. D. Electrolyte-gated transistors for organic and printed electronics. *Adv. Mater.* **2013**, *25*, 1822.

(13) Xia, Y.; Zhang, W.; Ha, M.; Cho, J. H.; Renn, M. J.; Kim, C. H.; Frisbie, C. D. Printed Sub-2 V Gel-Electrolyte-Gated Polymer Transistors and Circuits. *Adv. Funct. Mater.* **2010**, *20*, 587.

(14) Moon, H.; Seong, H.; Shin, W. C.; Park, W. T.; Kim, M.; Lee, S.; Bong, J. H.; Noh, Y. Y.; Cho, B. J.; Yoo, S.; Im, S. G. Synthesis of ultrathin polymer insulating layers by initiated chemical vapour deposition for low-power soft electronics. *Nat. Mater.* **2015**, *14*, 628.

(15) Ha, J. W.; Kim, Y.; Roh, J.; Park, J. I.; Kwak, J.; Lee, C.; Hwang, D. H. Thermally curable polymers consisting of alcohol-functionalized

DOI: 10.1021/acs.chemmater.7b03397
Chem. Mater. XXXX, XXX, XXX−XXX

cyclotetrasiloxane and melamine derivatives for use as insulators in OTFTs. *Org. Electron.* **2014**, *15*, 3666.
(16) Kim, K.; Kim, H.; Kim, S. H.; Park, C. E. Fluorinated polymer-grafted organic dielectrics for organic field-effect transistors with low-voltage and electrical stability. *Phys. Chem. Chem. Phys.* **2015**, *17*, 16791.
(17) Li, Y.; Wang, H.; Zhang, C. Y.; Zhang, Y. C.; Cui, Z. C.; Yan, D. H.; Shi, Z. S. Organic thin-film transistors with novel high-k polymers as dielectric layers. *Polym. Chem.* **2015**, *6*, 3685.
(18) Nketia-Yawson, B.; Kang, S. J.; Tabi, G. D.; Perinot, A.; Caironi, M.; Facchetti, A.; Noh, Y. Y. Ultrahigh Mobility in Solution-Processed Solid-State Electrolyte-Gated Transistors. *Adv. Mater.* **2017**, *29*, 1605685.
(19) Ha, Y. G.; Everaerts, K.; Hersam, M. C.; Marks, T. J. Hybrid Gate Dielectric Materials for Unconventional Electronic Circuitry. *Acc. Chem. Res.* **2014**, *47*, 1019.
(20) Ha, Y. G.; Emery, J. D.; Bedzyk, M. J.; Usta, H.; Facchetti, A.; Marks, T. J. Solution-Deposited Organic-Inorganic Hybrid Multilayer Gate Dielectrics. Design, Synthesis, Microstructures, and Electrical Properties with Thin-Film Transistors. *J. Am. Chem. Soc.* **2011**, *133*, 10239.
(21) Arnold, H. N.; Cress, C. D.; McMorrow, J. J.; Schmucker, S. W.; Sangwan, V. K.; Jaber-Ansari, L.; Kumar, R.; Puntambekar, K. P.; Luck, K. A.; Marks, T. J.; Hersam, M. C. Tunable Radiation Response in Hybrid Organic-Inorganic Gate Dielectrics for Low-Voltage Graphene Electronics. *ACS Appl. Mater. Interfaces* **2016**, *8*, 5058.
(22) Senanayak, S. P.; Sangwan, V. K.; McMorrow, J. J.; Everaerts, K.; Chen, Z. H.; Facchetti, A.; Hersam, M. C.; Marks, T. J.; Narayan, K. S. Self-Assembled Nanodielectrics for High-Speed, Low-Voltage Solution-Processed Polymer Logic Circuits. *Adv. Electron. Mater.* **2015**, *1*, 1500226.
(23) Everaerts, K.; Emery, J. D.; Jariwala, D.; Karmel, H. J.; Sangwan, V. K.; Prabhumirashi, P. L.; Geier, M. L.; McMorrow, J. J.; Bedzyk, M. J.; Facchetti, A.; Hersam, M. C.; Marks, T. J. Ambient-processable high capacitance hafnia-organic self-assembled nanodielectrics. *J. Am. Chem. Soc.* **2013**, *135*, 8926.
(24) De Vusser, S.; Genoe, J.; Heremans, P. Influence of transistor parameters on the noise margin of organic digital circuits. *IEEE Trans. Electron Devices* **2006**, *53*, 601.
(25) Beverina, L.; Ruffo, R.; Patriarca, G.; De Angelis, F.; Roberto, D.; Righetto, S.; Ugo, R.; Pagani, G. A. Second harmonic generation in nonsymmetrical squaraines: tuning of the directional charge transfer character in highly delocalized dyes. *J. Mater. Chem.* **2009**, *19*, 8190.
(26) Ha, Y. G.; Jeong, S.; Wu, J.; Kim, M. G.; Dravid, V. P.; Facchetti, A.; Marks, T. J. Flexible low-voltage organic thin-film transistors enabled by low-temperature, ambient solution-processable inorganic/organic hybrid gate dielectrics. *J. Am. Chem. Soc.* **2010**, *132*, 17426.
(27) Faessinger, R. W.; Brown, E. V. The Preparation of Pyridine Azo Compounds. *J. Am. Chem. Soc.* **1951**, *73*, 4606.
(28) Takeuchi, M.; Taguchi, M.; Shinmori, H.; Shinkai, S. Molecular design of boronic acid-based dye receptors for nucleosides. *Bull. Chem. Soc. Jpn.* **1996**, *69*, 2613.
(29) Mas, N.; Agostini, A.; Mondragón, L.; Bernardos, A.; Sancenón, F.; Marcos, M. D.; Martínez-Máñez, R.; Costero, A. M.; Gil, S.; Merino-Sanjuán, M.; Amorós, P.; Orzáez, M.; Pérez-Payá, E. Enzyme-Responsive Silica Mesoporous Supports Capped with Azopyridinium Salts for Controlled Delivery Applications. *Chem.—Eur. J.* **2013**, *19*, 1346.
(30) Maury, O.; Guegan, J. P.; Renouard, T.; Hilton, A.; Dupau, P.; Sandon, N.; Toupet, L.; Le Bozec, H. Design and synthesis of 4,4′-π-conjugated[2,2′]-bipyridines: a versatile class of tunable chromophores and fluorophores. *New J. Chem.* **2001**, *25*, 1553.
(31) Melanova, K.; Kovar, P.; Gamba, M.; Pospisil, M.; Benes, L.; Zima, V.; Svoboda, J.; Miklik, D.; Bures, F.; Knotek, P. Structural Arrangement of 4-[4-(Dimethylamino)phenylazo]pyridine Push-Pull Molecules in Acidic Layered Hosts Solved by Experimental and Calculation Methods. *Eur. J. Inorg. Chem.* **2017**, *2017*, 115.
(32) Demmer, C. S.; Krogsgaard-Larsen, N.; Bunch, L. Review on Modern Advances of Chemical Methods for the Introduction of a Phosphonic Acid Group. *Chem. Rev.* **2011**, *111*, 7981.
(33) Keglevich, G.; Grun, A.; Bolcskei, A.; Drahos, L.; Kraszni, M.; Balogh, G. T. Synthesis and Proton Dissociation Properties of Arylphosphonates: A Microwave-Assisted Catalytic Arbuzov Reaction with Aryl Bromides. *Heteroat. Chem.* **2012**, *23*, 574.
(34) Freedman, L. D.; Doak, G. O. The Preparation and Properties of Phosphonic Acids. *Chem. Rev.* **1957**, *57*, 479.
(35) Tian, M. Q.; Furuki, M.; Iwasa, I.; Sato, Y.; Pu, L. S.; Tatsuura, S. Search for squaraine derivatives that can be sublimed without thermal decomposition. *J. Phys. Chem. B* **2002**, *106*, 4370.
(36) Peor, N.; Sfez, R.; Yitzchaik, S. Variable Density Effect of Self-Assembled Polarizable Monolayers on the Electronic Properties of Silicon. *J. Am. Chem. Soc.* **2008**, *130*, 4158.
(37) Kobayashi, S.; Nishikawa, T.; Takenobu, T.; Mori, S.; Shimoda, T.; Mitani, T.; Shimotani, H.; Yoshimoto, N.; Ogawa, S.; Iwasa, Y. Control of carrier density by self-assembled monolayers in organic field-effect transistors. *Nat. Mater.* **2004**, *3*, 317.
(38) Pernstich, K. P.; Haas, S.; Oberhoff, D.; Goldmann, C.; Gundlach, D. J.; Batlogg, B.; Rashid, A. N.; Schitter, G. Threshold voltage shift in organic field effect transistors by dipole monolayers on the gate insulator. *J. Appl. Phys.* **2004**, *96*, 6431.
(39) Possanner, S. K.; Zojer, K.; Pacher, P.; Zojer, E.; Schürrer, F. Threshold Voltage Shifts in Organic Thin-Film Transistors Due to Self-Assembled Monolayers at the Dielectric Surface. *Adv. Funct. Mater.* **2009**, *19*, 958.
(40) Chung, Y.; Verploegen, E.; Vailionis, A.; Sun, Y.; Nishi, Y.; Murmann, B.; Bao, Z. A. Controlling Electric Dipoles in Nanodielectrics and Its Applications for Enabling Air-Stable n-Channel Organic Transistors. *Nano Lett.* **2011**, *11*, 1161.
(41) Shi, W.; Zheng, Y. F.; Yu, J. S.; Taylor, A. D.; Katz, H. E. Mobility enhancement of organic field-effect transistor based on guanine trap-neutralizing layer. *Appl. Phys. Lett.* **2016**, *109*, 143301.
(42) Horowitz, G.; Hajlaoui, R.; Bouchriha, H.; Bourguiga, R.; Hajlaoui, M. The concept of "threshold voltage" in organic field-effect transistors. *Adv. Mater.* **1998**, *10*, 923.
(43) Horowitz, G. Organic field-effect transistors. *Adv. Mater.* **1998**, *10*, 365.
(44) Xie, Y. T.; Cai, S. C.; Shi, Q.; Ouyang, S. H.; Lee, W. Y.; Bao, Z. A.; Matthews, J. R.; Bellman, R. A.; He, M. Q.; Fong, H. H. High performance organic thin film transistors using chemically modified bottom contacts and dielectric surfaces. *Org. Electron.* **2014**, *15*, 2073.
(45) Salinas, M.; Jager, C. M.; Amin, A. Y.; Dral, P. O.; Meyer-Friedrichsen, T.; Hirsch, A.; Clark, T.; Halik, M. The Relationship between Threshold Voltage and Dipolar Character of Self-Assembled Monolayers in Organic Thin-Film Transistors. *J. Am. Chem. Soc.* **2012**, *134*, 12648.
(46) Kraft, U.; Zschieschang, U.; Ante, F.; Kalblein, D.; Kamella, C.; Amsharov, K.; Jansen, M.; Kern, K.; Weber, E.; Klauk, H. Fluoroalkylphosphonic acid self-assembled monolayer gate dielectrics for threshold-voltage control in low-voltage organic thin-film transistors. *J. Mater. Chem.* **2010**, *20*, 6416.
(47) Zeng, Li.; Turrisi, R.; Fu, B.; Emery, J. D.; Walker, A. R.; Ratner, M. A.; Hersam, M. C.; Facchetti, A.; Marks, T. J.; Bedzyk, M. J. Manuscript in preparation.

DOI: 10.1021/acs.chemmater.7b03397
Chem. Mater. XXXX, XXX, XXX−XXX